Eur. Phys. J. D **35**, 31–42 (2005)
DOI: 10.1140/epjd/e2005-00062-4

THE EUROPEAN PHYSICAL JOURNAL D

Selected aspects of the quantum dynamics and electronic structure of atoms in magnetic microtraps

I. Lesanovsky[1,a] and P. Schmelcher[1,2,b]

[1] Physikalisches Institut, Universität Heidelberg, Philosophenweg 12, 69120 Heidelberg, Germany
[2] Theoretische Chemie, Institut für Physikalische Chemie, Universität Heidelberg, INF 229, 69120 Heidelberg, Germany

Received 4 February 2005 / Received in final form 18 March 2005
Published online 3 May 2005 – © EDP Sciences, Società Italiana di Fisica, Springer-Verlag 2005

Abstract. We analyze the quantum properties of atoms in a magnetic quadrupole field. The quantum dynamics of ground state atoms in this field configuration is studied firstly. We formulate the Hamiltonian and perform a symmetry analysis. Due to the particular shape of the quadrupole field in general there exist no stable states. We provide resonance energies, lifetimes and calculate the density of states and investigate under what conditions quasi-bound states occur that possess long lifetimes. An effective scalar Schrödinger equation describing such states is derived. As a next step we explore the influence of a high gradient quadrupole field on the electronic structure of excited atoms. An effective one-body approach together with the fixed nucleus approximation is employed in order to derive the electronic Hamiltonian. We present the energy spectrum and discuss peculiar features such as non-trivial spin densities and magnetic field induced electric dipole moments.

PACS. 03.75.Be Atom and neutron optics – 32.10.Dk Electric and magnetic moments, polarizability – 32.60.+i Zeeman and Stark effects

1 Introduction

In ultra cold atomic physics inhomogeneous magnetic fields have now being used for many years in order to manipulate and trap atoms. In conjunction with efficient cooling techniques such as evaporative cooling [1] even the occupation of the lowest quantum levels of magnetic traps became possible. This has paved the way to enter the regime of quantum degeneracy. Thus the exploration of phenomena such as Bose-Einstein condensation (see Ref. [2] and references therein) and the emergence of degenerate Fermi [3] gases became possible.

Apart from these collective phenomena the dynamics of single atoms is a major subject of current research [4–6]. The controlled manipulation of single atoms is an important step on the way to a quantum computer. The internal structure of atoms can be easily manipulated by external laser fields. This makes them promising systems for the realization of qubits which represent the information unit in quantum information processing. In order to realize a quantum register the atoms have to be individually addressable, i.e. their motion has to be confined to certain spatial areas. Moreover, the magnetic traps have to be designed such that a sufficiently long confinement of the atoms center of mass motion is provided. This qualifies the atom chip since its current carrying microstructures allow the generation of an almost arbitrary magnetic field configuration [7,8].

The microscopic size of the current carrying structures allows the generation of extremely high field gradients which would be never achievable with macroscopic setups. Hence the atom chip cannot only be used as a device for trapping and processing ground state atoms, and more generally matter waves, but also for the manipulation of the electronic structure of the atoms themselves: if highly excited atoms are exposed to such high gradient fields the common approach which is to treat an atom as a neutral point-particle essentially fails. Here rather the individual coupling of the atomic constituents with the external magnetic field has to be taken into account [9–11]. As we will show this leads to unique and surprising phenomena.

The paper is organized as follows: in Section 2 we analyze typical field configurations which can be realized by using the atom chip. Section 3 is dedicated to a detailed analysis of the motion electronic ground state atoms in a magnetic quadrupole trap. We introduce the Hamiltonian followed by a analysis of its symmetries. The resonance spectrum of atoms being trapped in a $F = 1$ hyperfine state and the density of states are provided. A scalar Schrödinger equation is derived which provides an approximative description of so-called quasi bound states. The results are applied to the case of ^{7}Li and ^{87}Rb atoms.

[a] e-mail: ilesanov@physi.uni-heidelberg.de
[b] e-mail: Peter.Schmelcher@pci.uni-heidelberg.de

In Section 4 we present an investigation of electronically excited atoms being exposed to a high gradient magnetic quadrupole field. By employing a fixed nucleus approximation we are led to an effective one-body Hamiltonian describing the electronic dynamics of the active electron of an alkali atom. After a brief symmetry analysis the spectral properties are investigated. The spin expectation values and in particular the spatial distribution of the spin polarization of electronically excited states are studied and analyzed in detail. The section concludes by investigating in detail the peculiar property of magnetic field-induced permanent electric dipole moments. Finally we provide our conclusions in Section 5.

2 Magnetic field configurations

The atom chip allows the generation of almost arbitrary magnetic field landscapes above its surface by combining external homogeneous fields with the inhomogeneous field created by the currents flowing in micron-sized wires on the chip [12,13]. However, despite this large variety, it turns out that there are only a few generic field configurations. These include two-dimensional quadrupole field (sideguide), the Ioffe-trap and the three-dimensional quadrupole field.

The sideguide is generated by a current carrying wire whose 'circular' magnetic field is superimposed by an external homogeneous bias field perpendicular to the direction of the current flow. As a result the field vanishes along a line parallel to the wire at a distance $\rho_0 = \mu_0 I/2\pi B$ being completely determined by the current I and the homogeneous magnetic field strength B. The Taylor expansion of the field around ρ_0 yields

$$\vec{B} \approx \frac{B}{\rho_0}\begin{pmatrix} x \\ -y \\ 0 \end{pmatrix} + \frac{B}{\sqrt{2}\rho_0^2}\begin{pmatrix} -x^2+2xy+y^2 \\ x^2+2xy-y^2 \\ 0 \end{pmatrix} + \frac{B}{\rho_0^3}\begin{pmatrix} y\left(y^2-3x^2\right) \\ -x\left(x^2-3y^2\right) \\ 0 \end{pmatrix}. \quad (1)$$

These are the quadrupolar, hexapolar and octopolar expansion terms of the field. Here we restrict ourselves to the linear term which should provide a good approximation for sufficiently large values of ρ_0. Thus we obtain the expression

$$\vec{B}_{2\mathrm{D}} = b\begin{pmatrix} x \\ -y \\ 0 \end{pmatrix}. \quad (2)$$

Here b is the magnetic field gradient determining the linear growth of the field with increasing distance from the line of zero field. To avoid the line of zero field this setup has to be slightly modified: By superimposing an additional homogeneous field along the z-direction a so-called Ioffe-trap is created.

Whereas the latter configurations only provide a two-dimensional confinement a so-called three-dimensional quadrupole field constitutes a trap in all three spatial dimensions. It is given by

$$\vec{B}_{3\mathrm{D}} = b\begin{pmatrix} x \\ y \\ -2z \end{pmatrix}. \quad (3)$$

In practice such a field is generated to a good approximation by a U-shaped wire [14]. In this investigation we exclusively study the structure and dynamics of atoms in the three-dimensional quadrupole field (3).

3 Center of mass motion of ground state atoms

In this section we investigate the resonant motion of atoms being trapped in a three-dimensional quadrupole trap. We assume that the atoms behave like neutral point-like particles which couple only through their total angular momentum to the magnetic field. This approximation is valid if the internal, i.e. electronic, structure effects are negligible which in particular holds for atoms in their electronic ground states. So far several authors have investigated the quantum behavior of neutral spin particles in a number of inhomogeneous field configurations: there have been studies regarding the wire trap [15–18], the magnetic guide and the Ioffe trap [19–21,11]. Except for the wire trap none of the latter allows for strictly bound states. For the latter even analytical results can be obtained if spin-$\frac{1}{2}$-particles and an infinitely thin wire are considered. In the context of cold neutron physics such solutions where obtained for the first time by Blümel and Dietrich by solving a fourth-order Hamburger equation [18]. Further investigations regarding the wire trap have been undertaken by Vestergaard Hau et al. [16] who have pursued a supersymmetric approach in order to obtain the Rydberg series of bound states. Particles of higher spin trapped by wires of a finite thickness have been investigated in the work by Burke et al. [17]. The quadrupole trap was first subject of investigation in a work by Bergeman et al. [22]. The authors have calculated about two dozens of resonances, i.e. the resonance energies and decay widths of spin-$\frac{1}{2}$-particles. Their numerical method is based on determining the phase shift of scattered waves.

In this section we formulate the Hamiltonian and calculate hundreds of resonances of spin-1-particles by utilizing the complex scaling method. We are therefore able to analyze and discuss global features of the resonance spectrum and the density of states. We also analyze under which conditions stable states can be achieved.

3.1 The Hamiltonian

The coupling to the external field is established by the interaction of the atomic magnetic moment with the magnetic field. The underlying Hamiltonian then becomes

$$H' = \frac{\vec{p}^{\,2}}{2M} - \vec{\mu}\cdot\vec{B}\left(\vec{r}\right) \quad (4)$$

with M and $\vec{\mu}$ being the mass and the magnetic moment of the atom, respectively. By assuming that the hyperfine splitting of the atomic energy levels is sufficiently large the hyperfine manifolds approximately decouple. Thus the quantum number F is approximately conserved. In each of the hyperfine-manifolds the magnetic moment can be represented by

$$\vec{\mu} = -\frac{g}{2}\vec{S} \tag{5}$$

with $\vec{S}$ being the spin-matrices of a spin-F-particle and g the respective g-factor. Inserting equation (3) the Hamiltonian becomes in atomic units[1]

$$H' = \frac{1}{2M}\left[\vec{p}^2 + b\,g\,M\,(x\,S_x + y\,S_y - 2z\,S_z)\right]. \tag{6}$$

All parameters in the Hamiltonian can be removed by introducing the scaled coordinates $\bar{x}_i = (bgM)^{\frac{1}{3}}\,x_i$ and $\bar{p} = (bgM)^{-\frac{1}{3}}\,p_i$. Omitting the bars the Hamiltonian becomes

$$M\,(bgM)^{-\frac{2}{3}}\,H' = H = \frac{1}{2}\left(\vec{p}^2 + x\,S_x + y\,S_y - 2z\,S_z\right). \tag{7}$$

Therefore the energy level spacing scales according to $(bgM)^{2/3}/M$.

3.2 Symmetries of the Hamiltonian

Before continuing we change the coordinate system to a cylindrical one ($\vec{r} \rightarrow (\rho, \phi, z)$) and employ the unitary transformation

$$U_1 = e^{-iS_z\phi}. \tag{8}$$

The Hamiltonian (7) becomes

$$\tilde{H} = U_1^+ H U_1 = \frac{1}{2}\Big[-\frac{\partial^2}{\partial\rho^2} - \frac{1}{\rho}\frac{\partial}{\partial\rho} + \frac{1}{\rho^2}(L_z - S_z)^2 - \frac{\partial^2}{\partial z^2} + \rho S_x - 2zS_z\Big]. \tag{9}$$

In the transformed frame the Hamiltonian does not contain an explicit dependence on the azimuthal angle ϕ. Thus the quantity L_z is conserved, i.e. $\left[\tilde{H}, J_z\right] = 0$. In order to see the physical meaning of L_z we transform back into the initial frame and find

$$U_1 L_z U_1^+ = L_z + S_z = J_z. \tag{10}$$

Thus the fact that L_z is conserved in the transformed frame is a direct consequence of the conservation of L_z in the initial frame, i.e. $[H, J_z] = 0$. Apart from rotations around the z-axis the Hamiltonian (9) is also invariant under the operation $\Sigma_x = P_z P_y e^{i\pi S_x}$, with P_z and P_y being the z- and y-parity operation. Since Σ_x and L_z anti-commute, i.e. $\{L_z, \Sigma_x\} = 0$ one can immediately show the existence of degeneracies in the spectrum.

Suppose $|E, m\rangle$ is an energy eigenstate of the Hamiltonian $\tilde{H}$ and at the same time an eigenstate of L_z with the quantum number m. Using the anti-commutator $\{L_z, \Sigma_x\} = 0$ one finds

$$L_z\Sigma_x\,|E, m\rangle = -\Sigma_x L_z\,|E, m\rangle = -m\Sigma_x\,|E, m\rangle\,. \tag{11}$$

Thus the state $\Sigma_x\,|E, m\rangle$ can be identified with $|E, -m\rangle$. Except for $m = 0$ these states form a degenerate pair since they possess the same energy. For a more detailed discussion of the symmetry properties we refer the reader to [9,10,23].

3.3 Resonances, decay widths, lifetimes and density of states

The three-dimensional quadrupole trap does not allow for strictly bound states: there is a point of zero field in the trap center causing so-called Majorana-spin flips which result in losses from the trap [25]. Thus the Hamiltonian (9) possesses rather a resonance than a bound spectrum.

We now specify our investigations to the case of spin 1, i.e. the atomic hyperfine state has to have the quantum number $F = 1$. In order to find the resonance spectrum of the Hamiltonian (9) we employ the complex scaling method. Here the phase space coordinates are rotated into the complex plane: $x_k \rightarrow x_k e^{i\eta}$ leading to a complex Hamiltonian. The complex scaling transformation does only affect continuum and not the bound states. Resonance states can become square integrable and at the same time their energy is rotated into the lower half of the complex energy plane [26]. In general the position of the complex energy will depend on the value of the scaling angle η: continuum states are rotated by an angle 2η from the real axis whereas energies belonging to resonance states once revealed maintain their positions. For such states the complex energy ε can be written as

$$\varepsilon = E - i\frac{\Gamma}{2}. \tag{12}$$

Here E and Γ are the energy and the decay width of the resonance, respectively. Therefore the lifetime τ of a certain resonance evaluates to $\tau = \Gamma^{-1}$.

In Figure 1 we present resonance energies and decay widths for several values of the quantum number m. For $m = 0$ and $m = 1$ one finds a triangular distribution of the resonances in the upper right of the $E - \Gamma$ plane. The resonances are placed on a series of diagonal lines with negative slope. The shape of the resonance pattern undergoes a significant alteration when reaching higher values of m. The pattern still exhibits a triangular shape, but the hypotenuse of it now possesses a positive slope. At the same time the arrangement of the resonances becomes increasingly regular.

[1] $\hbar = 1$, $m_e = 1$, $a_0 = 1$, $e = 1$: the magnetic gradient unit then becomes $b = 1$ a.u. $= 4.44181 \times 10^{15}$ T/m. The magnetic field strength unit is $B = 1$ a.u. $= 2.35051 \times 10^5$ T.

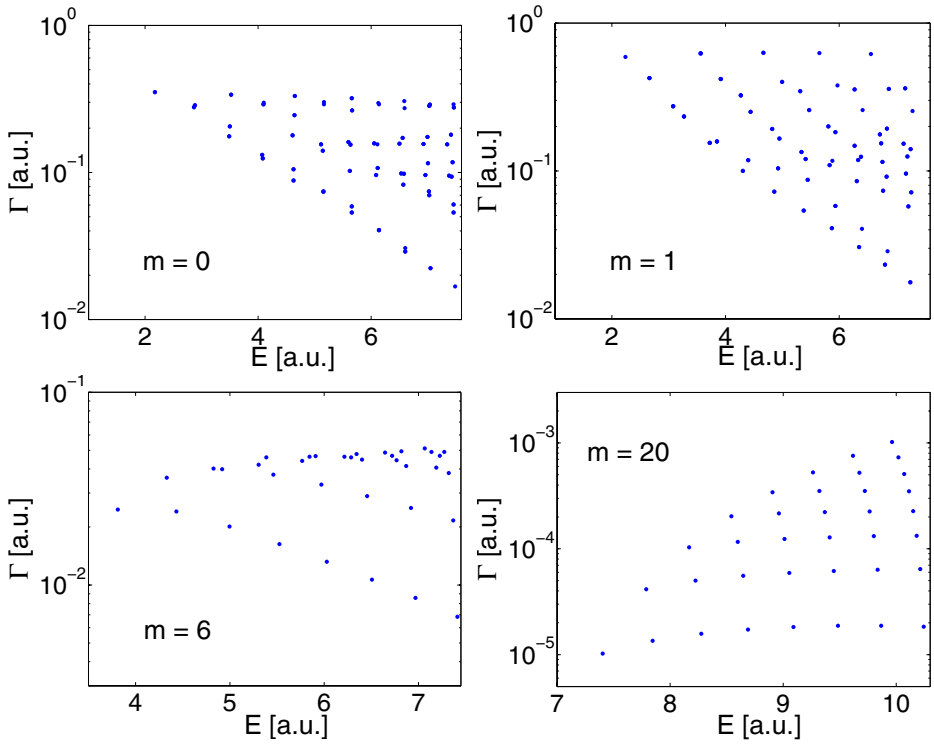

Fig. 1. Energies E and decay widths Γ (logarithmic scale) of resonances in the magnetic quadrupole trap for four values of the quantum number m. The structure of the resonance energy pattern undergoes a significant alteration with increasing m.

The density of states (DOS) profile $dN(E)_i/dE$ of a resonance state is determined by its energy E_i and the decay width Γ_i through [26]

$$\frac{dN}{dE}(E)_i = \frac{\Gamma_i}{\pi}\frac{1}{\Gamma_i^2 + (E-E_i)^2}. \tag{13}$$

The total density of states is obtained via

$$\frac{dN}{dE}(E) = \sum_i \frac{dN}{dE}(E)_i. \tag{14}$$

In Figure 2 we present the DOS for 4 selected values of the quantum number m. For $m = 0$ we observe broad peaks. The peaks of the DOS are determined by the resonances possessing the smallest decay width. The high background level is formed by short lived states. At $m = 5$ the energetically lowest resonance is well separated. At the same time a substructure becomes visible for energetically higher peaks. This substructure becomes manifest at $m = 10$ and at $m = 15$ extremely sharp peaks are formed. These sharp resonances are an indication for almost stable states. The peaks form clearly separated groups. The number of sub-peaks in adjacent groups differs by one.

Finally we want to investigate the decay width of the energetically lowest resonance in each m subspace. The corresponding behavior is presented in Figure 3. The decay width declines with increasing angular momentum. Performing an exponential fit we find $\Gamma \approx 0.68\, e^{-0.56|m|}$.

3.4 Quasi-bound states

In the preceding section we have found that the resonance states become increasingly stable the higher the angular momentum quantum number m is chosen. Thus it seems to be reasonable to expect that such states can be described as bound solutions of a given Schrödinger equation. In this section we will formulate such equation and analyze the quality of the provided approximation.

For large displacements from the trap center the interaction term of the magnetic moment with the magnetic field dominates the Hamiltonian. This term can be diagonalized applying the unitary transformation

$$U_2 = e^{-iS_y\beta} \tag{15}$$

with $\sin\beta = \rho/\sqrt{\rho^2+4z^2}$ and $\cos\beta = -2z/\sqrt{\rho^2+4z^2}$. The transformation performs a rotation in the spin space such that the z-component of the spin points into the local direction of the magnetic field vector. The interaction term now becomes

$$U_2^+(\rho S_x - 2zS_z)U_2 = \sqrt{\rho^2+4z^2}S_z = \left|\vec{\mathcal{B}}\right| S_z. \tag{16}$$

Since U_2 is a local, spatially dependent, transformation it also affects the derivatives. They transform as follows

$$U_2^+\frac{\partial^2}{\partial X^2}U_2 = \frac{\partial^2}{\partial X^2} - 2iS_y\frac{\partial\beta}{\partial X}\frac{\partial}{\partial X} - iS_y\frac{\partial^2\beta}{\partial X^2} - S_y^2\left(\frac{\partial\beta}{\partial X}\right)^2. \tag{17}$$

The derivatives of β can be evaluated by using the formula

$$\frac{\partial\beta}{\partial X} = -\frac{1}{\sin\beta}\frac{\partial\cos\beta}{\partial X}. \tag{18}$$

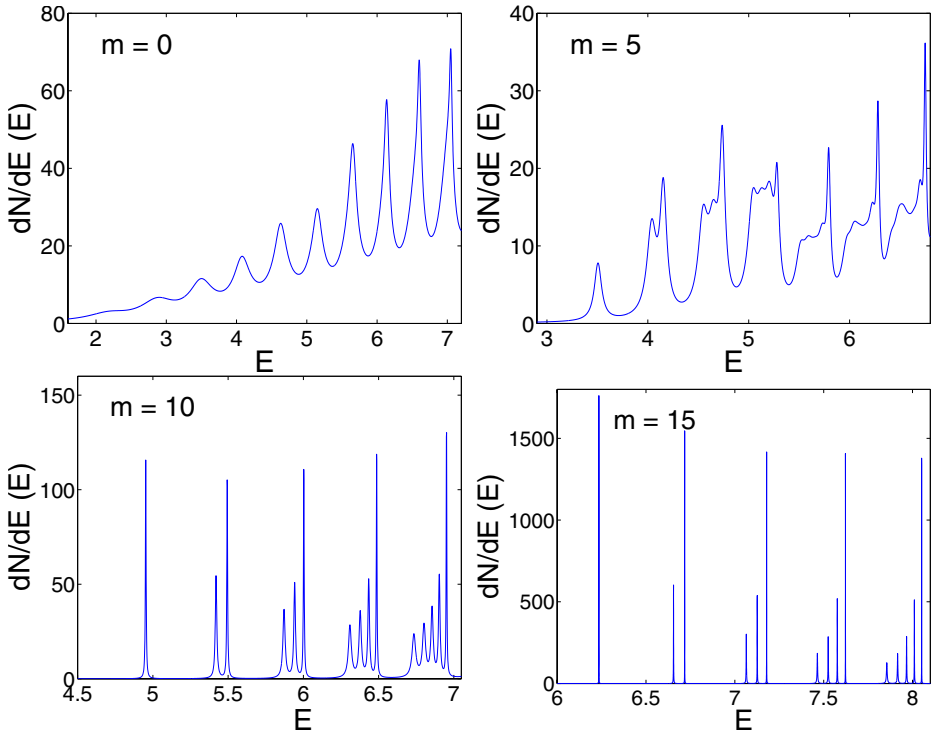

Fig. 2. Density of states for 4 selected values of the quantum number m. For small angular momentum the DOS is dominated by the longest living resonances which emerge from the high background level. Increasing angular momentum leads to a general decline of the decay width. Thus more peaks appear as the angular momentum increases. At the same time the background level decreases. At $m = 15$ one finds extremely narrow resonances which indicate extremely long-lived states.

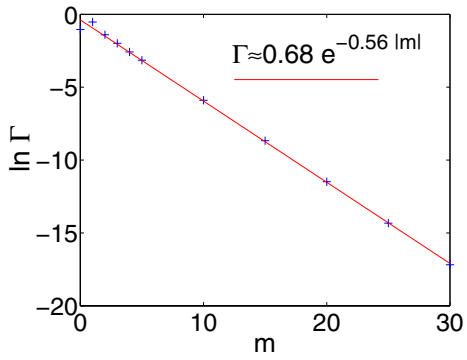

Fig. 3. Decay width of the energetically lowest resonance plotted against the quantum number m of the z-component of the total angular momentum. An exponential decrease of the decay width is observed. The increased stability of high m states originates from a localization of such states far away from the center of the trap.

Here X is used as a placeholder for the coordinates ρ and z. The Schrödinger equation resulting from the transformed Hamiltonian (9) now reads:

$$\frac{1}{2}\left[-\frac{\partial^2}{\partial\rho^2}-\frac{\partial^2}{\partial z^2}-\frac{1}{4\rho^2}+\frac{i2S_y}{|\vec{\mathcal{B}}|}\left(\cos\beta\frac{\partial}{\partial\rho}+2\sin\beta\frac{\partial}{\partial z}\right)+\frac{S_y^2}{|\vec{\mathcal{B}}|^2}(\cos^2\beta+4\sin^2\beta)+\frac{i6S_y\sin\beta\cos\beta}{|\vec{\mathcal{B}}|^2}+\frac{1}{\rho^2}(m-\cos\beta S_z+\sin\beta S_x)^2+S_z|\vec{\mathcal{B}}|\right]|\Phi\rangle=E|\Phi\rangle. \tag{19}$$

Note that we have introduced the wavefunction $|\Psi\rangle = \rho^{-\frac{1}{2}}|\Phi\rangle$ and replace L_z by its quantum number m. Although making the interaction term simpler it seems that nothing is gained since the kinetic term looks complicated. However, we now see that in the limit of very large displacements ($\rho\to\infty$) from the trap center the Schrödinger equation takes the form

$$\frac{1}{2}\left[-\frac{\partial^2}{\partial\rho^2}-\frac{\partial^2}{\partial z^2}+S_z\left|\vec{\mathcal{B}}\right|\right]|\Phi\rangle=E\,|\Phi\rangle\,. \tag{20}$$

Here S_z which now can be interpreted as the projection of the spin on the local direction of the magnetic field constitutes a conserved quantity. The projection quantum number m_s now defines whether trapping is possible at all. For $F=1$ only for $m_s=1$ trapped states can be expected. In order to find an approximate Schrödinger equation which describes this eventually bound states we project equation (19) onto the state $|+\rangle$ which is the eigenstate of S_z with the eigenvalue $m_s=1$. This yields

$$\frac{1}{2}\left[-\frac{\partial^2}{\partial\rho^2}-\frac{\partial^2}{\partial z^2}+\frac{m^2+\frac{3}{4}}{\rho^2}+\frac{4m\,z}{\rho^2\sqrt{\rho^2+4z^2}}-\frac{1}{2(\rho^2+4z^2)}+\frac{2(\rho^2+z^2)}{(\rho^2+4z^2)^2}+\sqrt{\rho^2+4z^2}\right]|\Phi_{qb}\rangle=E_{qb}\,|\Phi_{qb}\rangle\,. \tag{21}$$

The coupling terms we have neglected are proportional to powers of z^{-1} if $\rho\to 0$ and ρ^{-1} if $z\to 0$. Thus they become important only in the vicinity of the center of trap, where they lead to transitions between bound and unbound solutions. For large values of m the angular momentum barrier $(m^2+3/4)/\rho^2$ prevents the particle from

Table 1. Comparison of the resonance energies to the approximate energies E_{qb} obtained from equation (21). The first six resonance energies E for 5 selected values of the quantum number m are provided.

		0	1	2	3	4	5
	E	**2.1759**	**2.8639**	**2.8810**	**3.4898**	**3.5011**	**3.5233**
$m=0$	E_{qb}	2.0219	2.7252	2.7402	3.3725	3.3866	3.3900
	E	**2.2381**	**2.6590**	**3.0786**	**3.2702**	**3.5605**	**3.7222**
$m=1$	E_{qb}	2.0715	2.6180	2.9294	3.2149	3.4236	3.6123
	E	**3.5061**	**4.0377**	**4.1537**	**4.5472**	**4.6497**	**4.7384**
$m=5$	E_{qb}	3.4482	3.9775	4.0965	4.4890	4.5885	4.6856
	E	**6.2349**	**6.6549**	**6.7176**	**7.0645**	**7.1261**	**7.1789**
$m=15$	E_{qb}	6.2174	6.6408	6.6967	7.0527	7.1100	7.1545
	E	**8.4863**	**8.8483**	**8.9014**	**9.2043**	**9.2575**	**9.3042**
$m=25$	E_{qb}	8.4776	8.8409	8.8916	9.1978	9.2492	9.2932

Table 2. Energy unit, length unit as well as energy and lifetime of the ground state resonance for ^{7}Li ($2S_{1/2}$, $F=1$) and ^{87}Rb ($5S_{1/2}$, $F=1$) at a gradient $b=100$ T/m.

	energy unit [neV]	length unit [nm]	E_{gs} [neV]	τ_{gs} [μs]
^{7}Li	0.584	100.95	1.27	3.20
^{87}Rb	0.254	43.87	0.55	7.36

entering this region. In the following we will refer to the solutions of (21) as the quasi-bound states.

In Table 1 we present a comparison of the exact resonance energies to the quasi-bound energies E_{qb}. The energies show the expected behavior: for small angular momenta one finds larger discrepancies ($\Delta E/E = 0.07$ for the ground state in the $m=0$ subspace). However, as predicted, the approximation becomes significantly better if m is increased. The deviation of the ground state resonance in the $m=25$ subspace evaluates to $\Delta E/E = 1\times10^{-4}$.

3.5 Resonances of magnetically trapped alkali atoms

The results given in this paper can be directly applied to magnetically trapped alkali atoms. As instructive examples we choose the following two species: ^{7}Li being in the hyperfine ground state $2S_{1/2}$, $I=3/2$, $F=1$ and ^{87}Rb being in the hyperfine ground state $5S_{1/2}$, $I=3/2$, $F=1$. Here I and F denote the quantum numbers of $\vec{F}^2$ and $\vec{I}^2$, respectively. For the above hyperfine state we find for ^{87}Rb $g=1/2$ and $M=155798.23\,m_e$ and for ^{7}Li $g=1/2$ and $M=12789.55\,m_e$. In Table 2 we provide the energy and length unit as well as the energy E_{gs} and lifetime τ_{gs} of the ground state resonance at a gradient $b=100$ T/m. For this gradient the lifetimes are of the order of μs. The lifetime of trapped states can be significantly prolonged if the atom is prepared in states of high angular momentum. In case of ^{87}Rb (^{7}Li) being prepared in the $m=35$ subspace the minimum lifetime evaluates to 75.3 s (32.7 s).

4 Electronically excited atoms

In the first part of this paper we assumed that an atom can be approximated as a neutral point-like particle. This approximation is only valid if the variations of the external magnetic field are negligibly small throughout the atomic length scale. We will now concentrate on a thoroughly different regime, namely the structure of electronically excited atoms. By utilizing the benefits of the small structures of the atoms chips it is possible to generate magnetic fields which indeed vary significantly over typical size of such atoms. In such strong fields an atom can no more be treated as a point-like particle. Instead one has to take the various couplings of its individual components to the magnetic field into account. This gives rise to new phenomena such as non-trivial spin-polarizations which will be discussed in the following part of the paper. An extensive discussion of the electronic structure of atoms in quadrupolar magnetic fields can be found in [10,11,27].

4.1 The Hamiltonian

In our investigations we focus on atoms with a single active electron such as alkali atoms. Thereby, we assume the motion of the outermost (valence) electron to take place in a Coulomb potential of a single positive point charge, i.e. we assume the nuclear charge to be screened by the inner electron shells. For sufficient highly excited states this should provide a reasonable (approximate) description. We do not account for interactions arising from the non-Coulombic character of the core potential or relativistic effects such as spin-orbit coupling. Furthermore we neglect the coupling of the nuclear and electronic spin, i.e. the hyperfine interaction. Since the latter two interactions drop off as r^{-3} their treatment in terms of perturbation theory should be appropriate. The inclusion of the non-Coulombic nature of the core potential could be done via quantum defect theory and/or core pseudopotentials which goes beyond the scope of this paper.

The presence of an external magnetic field prevents the decoupling of the electronic and center of mass (c.m.) motion of the atom. This holds in particular for the

case of a homogeneous magnetic field [28–31] and has also to be expected for an inhomogeneous field. However, c.m. motional effects on the electronic structure become only significant in certain parameter and/or energetic regimes [32–34]. We take here advantage of the heavy atomic mass compared to the electron mass ($m_A \gg m_e = 1$). In addition we exploit the fact that we are dealing with ultra cold atoms whose c.m. motion takes place on much larger time scales than the electron dynamics, even for highly excited electronic states. We assume here that the atomic core (nucleus) is fixed in space at the trap center which coincides with the origin of the coordinate system. The Hamiltonian describing the electronic motion reads then

$$H_C = \frac{1}{2}\left(\vec{p} + \vec{A}(\vec{r})\right)^2 - \frac{1}{r} + \frac{g_s}{2}\vec{S}\vec{B}(\vec{r}). \tag{22}$$

Note, that unlike in the first part of this paper no scaled coordinates are used. A vector potential in the Coulomb gauge ($\nabla\vec{A}(\vec{r}) = 0$) belonging to the quadrupole field (3) reads

$$\vec{A}(\vec{r}) = \frac{1}{3}\left[\vec{B}(\vec{r}) \times \vec{r}\right] = b\begin{pmatrix} yz \\ -xz \\ 0 \end{pmatrix}. \tag{23}$$

Inserting the expressions (3) and (23) into the Hamiltonian (22) yields

$$H_C = -\frac{1}{2}\Delta - \frac{1}{\sqrt{x^2+y^2+z^2}} - b\,zL_z + \frac{b^2}{2}z^2\left(x^2+y^2\right) + \frac{b}{2}\left(\sigma_x x + \sigma_y y - 2\sigma_z z\right). \tag{24}$$

Here we have set the electronic g-factor to $g_s = 2$. L_z is the z component of the orbital angular momentum operator, and σ_x, σ_y, σ_z are the Pauli spin matrices ($\vec{S} = \frac{1}{2}\vec{\sigma}$). The third and fourth term of H_C originate from the charge coupling to the external field. The paramagnetic ($\propto b$) or Zeeman term depends not only on L_z but also linearly on the z-coordinate. The diamagnetic term ($\propto b^2$) represents a quartic oscillator coupling term between the cylindrical coordinates $\rho = \sqrt{x^2+y^2}$ and z. The final term of H_C originates from the coupling of the magnetic moment of the spin of the valence electron to the magnetic field. It depends linearly on the gradient and prevents the factorization of the motions in the spin and spatial degrees of freedom. Thus the corresponding Schrödinger equation is rendered into a spinor equation. In the case of a homogeneous field the spin dynamics can be decoupled from the spatial motion which leads to a scalar Schrödinger equation. This non-trivial spin-field coupling term is essential for the emergence of a plethora of new effects such as the emergence of magnetic field induced electric dipole moments.

4.2 Symmetries of the Hamiltonian

For the following investigations it is appropriate to transform the Hamiltonian (24) employing spherical coordinates. It then reads

$$H_S = -\frac{1}{2}\Delta_{r,\theta,\phi} - \frac{1}{r} + \frac{b^2}{2}r^4\cos^2\theta\sin^2\theta + \frac{b}{2}r\sin\theta\,K - b\,r\cos\theta\,(L_z + \sigma_z) \tag{25}$$

with K being the matrix

$$K = \begin{pmatrix} 0 & e^{-i\phi} \\ e^{i\phi} & 0 \end{pmatrix}. \tag{26}$$

Like the Hamiltonian (7) we find H_S to be invariant under rotations around the z-axis. Hence we find $[H_S, J_z] = 0$. Moreover we find another symmetry of the system, namely $P_y P_z \sigma_x$. This quantity anti-commutes with J_z, i.e. $\{J_z, P_y P_z \sigma_x\} = 0$. Using the same argument as in Section 3.2 one can show, that the states $|E, m\rangle$ and $P_y P_z \sigma_x |E, m\rangle = |E, -m\rangle$ form a degenerate pair. Since J_z can only assume half-integer values this degeneracy is found for any electronic state.

4.3 Energy spectrum

The eigenvalue problem of the Hamiltonian (25) is obtained by using the linear variational principle with a Sturmian basis set. In order to estimate the convergence behavior of the eigenstates we at first calculate a number of eigenvalues $E_i^{G_1}$ for a given basis set size G_1. Afterwards the basis size is significantly increased to a value G_2 and the calculation is performed again yielding the new set of eigenvalues $E_i^{G_2}$. As a measure of convergence we then define the quantity

$$K_i = \left|\frac{E_i^{G_1} - E_i^{G_2}}{E_i^{G_1} - E_{i-1}^{G_1}}\right| \tag{27}$$

where the difference of the same eigenvalue for the two basis sizes G_1 and G_2 is divided by the distance to the lower neighboring eigenvalue. For $K_i \leq 0.01$ we consider the eigenvalue $E_i^{G_2}$ to be well converged. In our calculations we have employed basis sets with dimensions up to 17,000 (in case of a homogeneous magnetic field even more than 100,000). We thereby were able to converge several thousand eigenstates and eigenvalues up to energies corresponding to a principal quantum number of $n \approx 60$ with J_z-quantum numbers $m\,\epsilon\,[-7/2, 7/2]$. A thorough discussion of this procedure is found in [27].

Starting from $b = 0$ the energy spectrum undergoes significant changes with increasing gradient. Essentially one can distinguish three regimes which are the weak, the intermediate and the strong gradient regime. Of course, these regimes are not only determined by the absolute value of the gradient b but also by the degree of excitation of the atom. Thus it is natural to define the weak/strong regime to be the regime, for which the magnetic compared to the Coulomb interaction is weak/strong [35]. For weak gradients the behavior of the energy levels is dominated

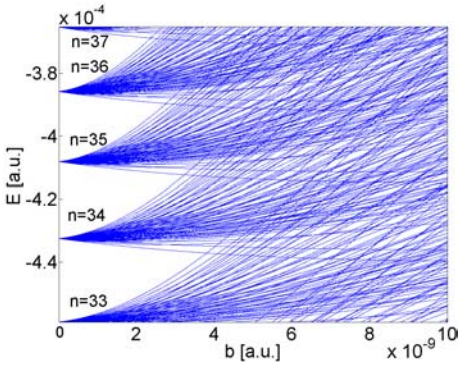

Fig. 4. Energy spectrum of the multiplets $n = 33-37$ for the states with $m = \pm 1/2$. For low gradients the energy levels split almost linearly followed by a transition region where the diamagnetic term becomes increasingly more important. For high gradients different n-multiplets overlap and no symmetries, i.e. approximate quantum numbers, are left.

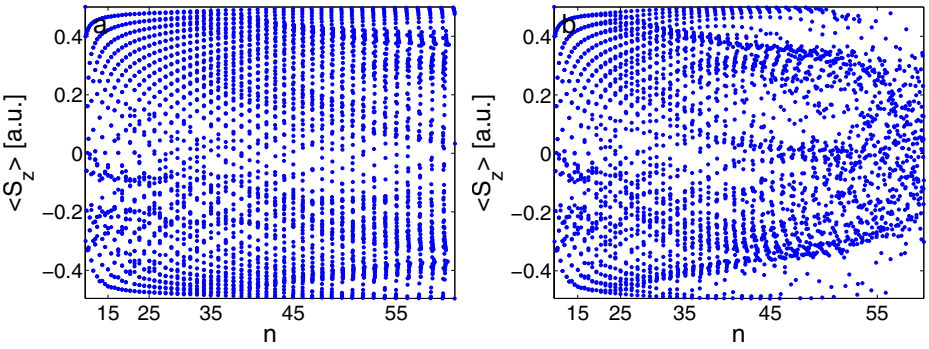

Fig. 5. Expectation values of the z-component of the spin operator as a function of the quantum number n for different gradients (a: $b = 10^{-10}$, b: $b = 10^{-9}$) in the $m = 3/2$ subspace.

by the orbital and spin Zeeman terms both of which depend linearly on the gradient. We find a linear splitting of the degenerate n-multiplets with increasing b. Adjacent n-multiplets do not overlap which makes n an almost good quantum number.

With increasing gradient the diamagnetic term with its quadratic dependence on b gains in importance resulting in a non-linear behavior of the energy curves. The intra n-manifold mixing regime scales $b \propto n^{-6}$. In this regime different n-multiplets are still energetically well separated but different angular momentum states (l-states) mix. For even higher gradients we observe mixing of different n-multiplets which leads to the global emergence of avoided crossings. The onset of this inter n-manifold mixing scales according to $b \propto n^{-11/2}$ whereas in a homogeneous field one finds $B \propto n^{-7/2}$. In Figure 4 we show the energy levels of n-multiplets ranging from $n = 33$ to $n = 37$ with $m = \pm\frac{1}{2}$ in the regime $0 \leq b \leq 10^{-8}$. For such a degree of excitation the intra n-manifold mixing sets in at $b \approx 5 \times 10^{-10}$. Therefore the linear splitting due to the Zeeman-term is hardly visible. For $b = 8 \times 10^{-9}$ we are deep inside the inter-n-mixing regime.

4.4 Properties of the electronic spin

4.4.1 Expectation values

For an atom being exposed to a homogeneous magnetic field pointing into z-direction the z-component of the electronic spin S_z yields a conserved quantity. In this case, the electronic wavefunctions can be chosen to be eigenfunctions of S_z. Hence the expectation value $\langle S_z \rangle$ can only assume one of the two values $\pm\frac{1}{2}$. Due to the non-trivial spin-field interaction term S_z constitutes no conserved quantity if a quadrupole field is present. In Figure 5 we present the distribution of $\langle S_z \rangle$ for electronic states of the $m = \frac{3}{2}$ subspace as a function of the effective principal quantum number $n = \sqrt{-1/2E}$ [2]. Since S_z is not conserved the values of $\langle S_z \rangle$ cover the complete interval $[-1/2, 1/2]$. In Figure 5a ($b = 10^{-10}$) one observes a regular distribution of the expectation values as long as $|\langle S_z \rangle| > 0.3$. The dots with largest $\langle S_z \rangle$ correspond to the so-called ellipsoidal states [27] which possess large mean orbital angular momentum and are almost completely spin polarized. In contrast to this the states corresponding to the smallest values of $\langle S_z \rangle$ show a small expectation value of the orbital angular momentum. Around $\langle S_z \rangle = 0$ the distribution of the expectation values appears to be irregular and less dense. Unlike this one would encounter an overall regular and even distribution if the $m = 1/2$ subspace was considered [10]. For low n the values of $\langle S_z \rangle$ form vertical lines which originate from the approximate degeneracy of the energy levels. When reaching higher degrees of excitation these lines widen. For $b = 10^{-10}$ we do not find significant inter-n-mixing up to $n = 60$. Thus, all lines in Figure 5a are well separated. For larger gradients $b = 10^{-9}$ (Fig. 5b) the above-discussed properties are equally present for low-lying states. However, with increasing excitation energy we enter the inter-n-mixing regime at $n \approx 35$. Here any regular structure is dissolved and an overall irregular distribution of $\langle S_z \rangle$ values appears. For $\langle S_z \rangle > 55$ the distribution narrows significantly. Here the occupied interval is approximately $[-0.3, 0.3]$.

[2] Since an external magnetic field is present n is not a genuine quantum number. It can also assume fractional values.

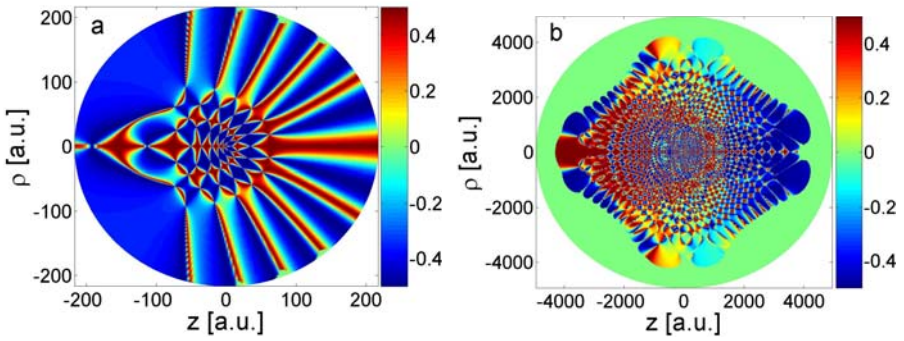

Fig. 6. (a) S_z-polarization of an electronic state whose energy corresponds to an effective principal quantum number of $n = 9$. The state is located in the $m = \frac{1}{2}$-subspace. The magnetic field gradient is $b = 10^{-9}$. (b) S_z-polarization of an highly excited state. With an effective quantum number $n = 44.29$ its situated in the inter-n-mixing regime. The values for m and b are the same is in (a). A colour version of the figures is available in electronic form at `http://www.eurphysj.org`.

4.4.2 Spin polarization

As already pointed out the non-trivial coupling of the spin to the spatial degrees of freedom prevents the factorization of the wavefunction into a spatial and a spin part. Hence, the orientation of the electronic spin is expected to depend on the spatial position of the electron. To study this in more detail we introduce the S_z-polarization $W_S(\vec{r})$. For a J_z-eigenstate $|E, m\rangle$ it reads

$$W_S(\vec{r}) = \frac{\langle E, m|\vec{r}\rangle\, S_z\, \langle \vec{r}|E, m\,\rangle}{\langle E, m|\vec{r}\rangle\, \langle \vec{r}|E, m\,\rangle}. \qquad (28)$$

In Figure 6 we present the S_z-polarization of two excited states. The first one (Fig. 6a) has an effective principal quantum number of $n = 9$ and is located in the $m = \frac{1}{2}$-subspace. The magnetic field gradient is $b = 10^{-9}$. We observe a complex pattern of domains exhibiting different spin orientation (red: spin up, blue: spin down). If the spin and the spatial part of the wavefunction factorized as it is the case for homogeneous field we would encounter a spatially uniform distribution. For small displacements from the coordinate center we observe the domains to form a pattern similar to that of a chess board. With increases distance we encounter a transition region where the formation of stripes with different spin orientation sets in. The junctions where four spin domains meet each other coincide with the nodes of the spatial probability density. Our investigation revealed that both the Coulomb interaction and the spin-Zeeman term are responsible for the formation of the interwoven network of islands exhibiting different spin orientation. The additional presence of the orbital Zeeman and the diamagnetic term only results in a deformation of this network. In Figure 6a we show another S_z-polarization but for a much higher excited state which an effective principal quantum number of $n = 44.29$. This state is already affected by the inter-n-mixing. The pattern exhibits a more complex structure. This is expected since the number of nodes in the wavefunction is determined by the degree of excitation. Apparently, the distribution of the spin polarized islands for this state is not symmetric: For negative/positive z values a dominance of red/blue colored regions is evident. This feature can be understood by investigating a Hamiltonian exclusively consisting of the spin Zeeman term:

$$\hat{H}_S = -\vec{\mu}\,\vec{B}(\vec{r}) = \frac{b}{2} r \begin{pmatrix} -2\cos\theta & \sin\theta\, e^{-i\phi} \\ \sin\theta\, e^{i\phi} & 2\cos\theta \end{pmatrix}. \qquad (29)$$

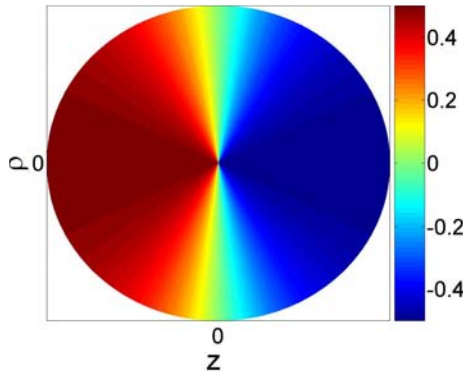

Fig. 7. S_z-polarization of the eigenstate $\Phi_+(r, \theta, \phi)$ of the Hamiltonian (29). The electronic spin either points antiparallel (W_S^+) or parallel ($W_S^- = -W_S^+$) to the local direction of the field. A colour version of the figure is available in electronic form at `http://www.eurphysj.org`.

Here the complete dynamics takes place in spin space since the spatial coordinates (r, θ, ϕ) are entering as parameters. The Hamiltonian (29) is diagonalized by the transformation $U_1 U_2$ where U_1 and U_2 are given through equations (8) and (15), respectively. Its two solutions are

$$\begin{aligned} \Phi_-(r, \theta, \phi) &= U_2^+ U_1^+ \,|\uparrow\rangle \\ \Phi_+(r, \theta, \phi) &= U_2^+ U_1^+ \,|\downarrow\rangle \end{aligned} \qquad (30)$$

with $|\uparrow\rangle$ and $|\downarrow\rangle$ being the eigenstates of the spin-operator S_z. The corresponding eigenenergies are

$$E_\pm = \mp\frac{1}{2} b\, r \sqrt{1 + 3\cos^2\theta} = \mp|\vec{\mu}||\vec{B}(\vec{r})|. \qquad (31)$$

These energies correspond to those of a spin oriented parallel (E_-) or antiparallel (E_+) to the magnetic quadrupole field. Constructing the S_z-polarization $W_S^\pm$ of the eigenstates (30) yields

$$W_S^\pm = \pm\frac{1}{2}\cos\beta = \mp\frac{z}{\sqrt{\rho^2 + z^2}} = \mp\frac{\cos\theta}{\sqrt{1 + 3\cos^2\theta}}. \qquad (32)$$

The S_z-polarization W_S^+ shown in Figure 7. Both, W_S^+ and $W_S^- = -W_S^+$ neither depend on the radial coordinate nor on the azimuthal angle ϕ. For negative values of z the z-component of the spin is oriented upwards/downwards

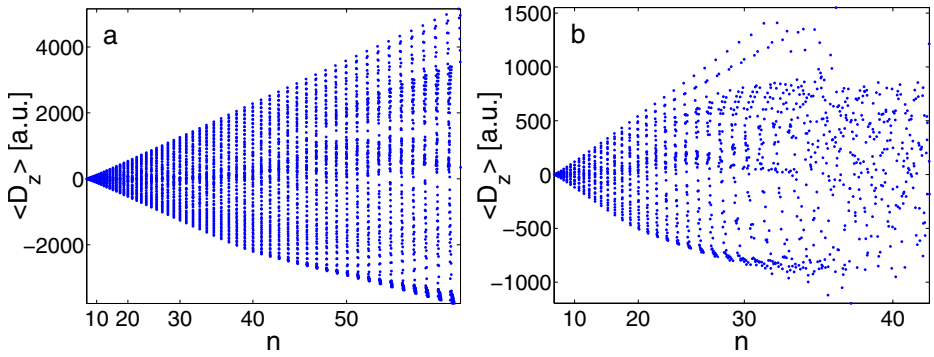

Fig. 8. Expectation value of the dipole operator D_z plotted versus the principle quantum number n for different gradients (a: $b = 10^{-10}$, b: $b = 10^{-8}$). The states lie in the $m = 3/2$ subspace.

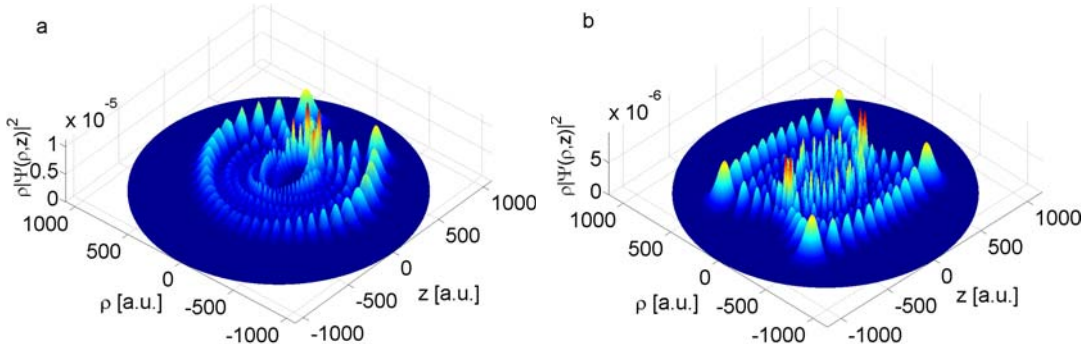

Fig. 9. (a) Charge distribution of an electronic state in a quadrupole field ($b = 10^{-8}$). The state belongs to the $n = 21$-multiplet in the $m = 1/2$ subspace. The asymmetric charge distribution with respect to the $z = 0$-line gives rise to a permanent electric dipole moment. (b) Charge distribution for an electronic state ($n \approx 21$, $m = 1/2$) in a homogeneous field $\vec{B}_H = B\vec{e}_z$ ($B = 10^{-6}$). The electron cloud is mirror symmetric with respect to both the $z = 0$- and $\rho = 0$-line. Thus, no permanent electric dipole moment occurs. A colour version of the figures is available in electronic form at `http://www.eurphysj.org`.

whereas the opposite orientation is found for positive z values. Around the z-axis there is a transition region with $W_S^{\pm}$ being close to zero.

This is precisely the behavior we have observed at large r for the S_z-polarization of the highly excited state depicted in Figure 6b. Apparently in this particular state the electron spin prefers an antiparallel alignment with respect to the external field at large radii which corresponds to W_S^+. This situation is to some extend reminiscent of the quasi-bound states which have been discussed in Section 3.4. Here the far away from the trap center the magnetic field interaction dominates the Hamiltonian and the projection of the particles spin on the local direction of the magnetic field is conserved.

4.5 Magnetic field induced electric dipoles

For an atom in a homogeneous field (and also in the field free case) parity is a symmetry. Thus electronic states do not exhibit a permanent electric dipole moment: $\langle \vec{D} \rangle = \langle \vec{r} \rangle = 0$. In this subsection we investigate the electric dipole moment of the electronic states of an atom in the quadrupole field. Due to the rotational invariance of the system the expectation values $\langle x \rangle$ and $\langle y \rangle$ vanish. However, the expectation value of $D_z = z$ is in general non-zero. It is shown in Figure 8 for the two gradients $b = 10^{-10}$ and $b = 10^{-8}$, respectively. Similar to the S_z expectation value (see Sect. 4.4) we find the electric dipole moments which belong to the almost degenerate states of an n-multiplet to be arranged along vertical lines. Within a given n-multiplet the dipole moments vary within an upper and a lower bound. In the absence of inter-n-mixing both of these bound depend approximately linearly on n. States with a large electric dipole moment emerge from field-free states (with increasing b) that possess small values for the angular momentum and vice versa. For $b = 10^{-8}$ and $n > 35$ the distribution of the dipole moments becomes completely irregular.

We have shown the remarkable effect that the external magnetic quadrupole field induces a state dependent permanent electric dipole moment. This is the result of an asymmetric charge density distribution induced by the symmetry properties of the quadrupole field. Figure 9a exemplarily shows the density distribution of an electronic state inside a quadrupole field. The electronic cloud is almost completely localized in the $z > 0$ half-space which results in a large dipole moment. In contrast to that one finds for states inside a homogeneous field $\vec{B}_H = B\vec{e}_z$ a symmetric charge distribution (see Fig. 9b).

In particular in the context of Quantum Information Processing the emergence of state dependent electric dipole moments seems be an interesting phenomenon.

In order to build a working two qubit gate one is interested in finding ways to establish a controlled interaction between two qubits to gain a phase shift. Considering a trapped Rydberg state as a qubit the interaction between two of them can be realized via dipole-dipole interaction. The magnitude of this interaction could be tuned at will just by changing the atomic state in the quadrupole field.

5 Conclusion

In the first part of this paper we have analyzed the quantum dynamics of atoms in a 3D magnetic quadrupole field. The atoms are hereby treated as point particles carrying a specific angular momentum, i.e. magnetic moment. We have set up the Hamiltonian and performed an analysis of its symmetry properties. In this context we have proven the existence of degeneracies in the resonance spectrum of the system.

The resonance spectrum of atoms being trapped in a $F = 1$ hyperfine state has been presented. The resonance energies for a wide range of values of the quantum number m is discussed and the distribution of the resonance positions in the $E - \Gamma$ plane is analyzed. For low m values we have found a triangular shaped pattern exhibiting both regular and irregular regions. For large angular momenta the transition of the resonance positions to a regular pattern is observed. From the resonance data we have calculated the density of states. For small m values the DOS is dominated by a few peaks on top of a strong background. The width of these peaks decreases if the angular momentum is increased. With increasing m the DOS becomes more structured until sharp peaks emerge which indicate long-lived states.

We have further shown that there is an exponential increase with respect to the lifetimes of the resonance states with increasing angular momentum. We have shown that transitions between bound and unbound solutions take place only in the vicinity of the trap center and are therefore highly suppressed for large angular momentum states. The latter quasi-bound states, which possess long lifetimes, can be very well described by a scalar radial Schrödinger equation. Its approximate eigenenergies are in good agreement with the resonance energies obtained from the complex scaling calculation and become exact in the limit of high m quantum numbers.

The results have been applied to ^{87}Rb and ^{7}Li being trapped in a $F = 1$ hyperfine state. We have shown that lifetimes of the order of minutes can be achieved for sufficient large values of the angular momentum.

In the second part of this paper we investigate the electronic structure of electronically highly excited hydrogen-like atoms assuming an infinitely heavy nucleus that is fixed at the center of the trap. We have pursued an one-particle approach in order to describe the dynamics of the valence electron of the excited atom. Here we have considered both the coupling of the electric charge and the magnetic moment (spin) to the field. The inhomogeneous character of the quadrupole field results in a coupling of the spatial and spin degrees of freedom. As a result of this unique coupling the system is invariant under a number of symmetry operations acting on both degrees of freedom. We have found unitary symmetries relying on the conservation of the total angular momentum J_z and the discrete operation $P_y P_z \sigma_x$. Here we could also prove the presence of a two-fold degeneracy in the energy spectrum. We have provided scaling relations for the onset of both the intra- and the inter-n-manifold mixing in a quadrupole field. Modifications of the energy spectrum especially due to scattering with the inner electron shells have not been considered. Effects basing on the latter can be understood by quantum defect theory [36,37]. At least for Rydberg states which possess a large angular momentum we do not expect significant changes induced by core scattering processes.

The system is numerically solved by using the linear variational principle employing a Sturmian basis set. We present the energy spectrum and discuss its particular appearance in the weak, intermediate as well as the strong gradient regime.

Analyzing the electronic spin properties we have found the S_z-expectation values of the electronic states to form a regular pattern at low gradients. At higher gradients or higher excitation, respectively, the regular structure is replaced by a much narrower irregular distribution. To investigate of the local spin orientation we have introduced the S_z-polarization. For electronic states in the quadrupole field this quantity reveals a rich nodal structure which originates from the unique coupling of the spin and spatial degrees of freedom. The chess-board-like structure consisting of islands with alternating spin orientations at low radii is replaced by striped pattern as the radius increases. For Rydberg states we have found a spin polarization effect taking place in the asymptotic region. Here the S_z-polarization exhibits a global dependence on the z-coordinate. This has been analyzed by studying a Hamiltonian which exclusively describes the coupling of the electronic spin to the magnetic field. Calculating its eigenstates analytically we could reproduce the above mentioned z-dependence of the S_z-polarization of Rydberg-states for large radii.

By calculating the expectation value of the dipole operator we have found it to be non-zero in general. This is unlike the situation in the homogeneous field where the conservation of parity prevents the emergence of permanent dipole moments. For low degrees of excitation and low gradients we observe an almost linear increase of the maximum dipole moment within a n-manifold. The previously regular pattern becomes increasingly distorted when moving to higher gradients and/or a higher degree of excitation. We have found the non-vanishing dipole moment to be a direct consequence of the symmetry properties of the quadrupole field which force an asymmetric electronic charge distribution with respect to the $x - y$-plane.

Financial support of the Deutsche Forschungsgemeinschaft and fruitful discussions with Jörg Schmiedmayer are gratefully acknowledged.

References

1. H.J. Metcalf, P. van der Straten, *Laser Cooling and Laser Trapping* (Springer Verlag, New York, 1999)
2. C.J. Pethick, H. Smith, *Bose-Einstein Condensation in Dilute Gases* (Cambridge University Press, 2002)
3. F. Schreck et al., Phys. Rev. Lett. **87**, 080403 (2001)
4. J. Ye, D.W. Vernooy, H.J. Kimble, Phys. Rev. Lett. **83**, 4987 (1999)
5. P. Horak et al., Phys. Rev. Lett. **88**, 043601 (2002)
6. D. Schrader et al., Phys. Rev. Lett. **93**, 150501 (2004)
7. J. Reichel, W. Hänsel, T. W. Hänsch, Phys. Rev. Lett. **83**, 3398 (1999)
8. R. Folman et al., Phys. Rev. Lett. **84**, 4749 (2000)
9. I. Lesanovsky, J. Schmiedmayer, P. Schmelcher, Europhys. Lett. **65**, 478 (2004)
10. I. Lesanovsky, J. Schmiedmayer, P. Schmelcher, Phys. Rev. A **69**, 053405 (2004)
11. I. Lesanovsky, J. Schmiedmayer, P. Schmelcher, Phys. Rev. A **70**, 043409 (2004)
12. R. Folman et al., Adv. At. Mol. Opt. Phys. **48**, 263 (2002)
13. J. Reichel, Appl. Phys. B **74**, 469 (2002)
14. S. Wildermuth et al., Phys. Rev. A **69**, 030901(R) (2004)
15. K. Berg-Sorensen et al., Phys. Rev. A **53**, 1653 (1996)
16. L. Vestergaard Hau, J.A. Golovchenko, M.M. Burns, Phys. Rev. Lett. **75**, 1426 (1995)
17. J.P. Burke Jr, C.H. Greene, B.D. Esry, Phys. Rev. A **54**, 3225 (1996)
18. R. Blümel, K. Dietrich, Phys. Rev. A **43**, 22 (1991)
19. E.A. Hinds, C. Eberlein, Phys. Rev. A **61**, 033614 (2000)
20. E.A. Hinds, C. Eberlein, Phys. Rev. A **64**, 039902(E) (2000)
21. R.M. Potvliege, V. Zehnlé, Phys. Rev. A **63**, 025601 (2001)
22. T.H. Bergeman et al., J. Opt. Soc. Am. B **6**, 2249 (1989)
23. I. Lesanovsky, P. Schmelcher, Phys. Rev. A **71**, 032510 (2005)
24. I. Lesanovsky, P. Schmelcher, Phys. Rev. A **70**, 063604 (2004)
25. C.V. Sukumar, D.M. Brink, Phys. Rev. A **56**, 2451 (1997)
26. N. Moiseyev, Phys. Rep. **302**, 5 (1998)
27. I. Lesanovsky, P. Schmelcher, J. Phys. B: At. Mol. Opt. Phys. **38**, S151 (2005)
28. W.E. Lamb, Phys. Rev. **85**, 259 (1959)
29. J.E. Avron, I.W. Herbst, B. Simon, Ann. Phys. (N.Y.) **114**, 431 (1978)
30. B.R. Johnson, J.O. Hirschfelder, K.H. Yang, Rev. Mod. Phys. **55**, 109 (1983)
31. P. Schmelcher, L.S. Cederbaum, U. Kappes, *Conceptual Trends in Quantum Chemistry*, edited by E.S. Kryachko, J.L. Calais (Kluwer Academic Publishers, 1994), pp. 1-51
32. H. Ruder et al., *Atoms in Strong Magnetic Fields* (Springer, 1992)
33. P. Schmelcher, L.S. Cederbaum, Phys. Lett. A **164**, 305 (1992)
34. O. Dippel, P. Schmelcher, L.S. Cederbaum, Phys. Rev. A **49**, 4415 (1994)
35. H. Friedrich, D. Wintgen, Phys. Rep. **183**, 37 (1989)
36. *Atoms and Molecules in Strong External Fields*, edited by P. Schmelcher, W. Schweizer (Plenum Press, 1998)
37. Q. Wang, C.H. Greene, Phys. Rev. A **44**, 1874 (1991)